

ARTICLE

Astrocyte-derived TNF and glutamate critically modulate microglia activation by methamphetamine

Teresa Canedo^{1,2,9}, Camila Cabral Portugal^{3,9}, Renato Socodato³, Tiago Oliveira Almeida^{3,4}, Ana Filipa Terceiro^{1,4}, Joana Bravo^{1,4}, Ana Isabel Silva^{1,4}, João Duarte Magalhães¹, Sónia Guerra-Gomes⁵, João Filipe Oliveira^{6,7}, Nuno Sousa^{5,6}, Ana Magalhães^{1,4}, João Bettencourt Relvas^{2,3} and Teresa Summavielle^{1,8}

© The Author(s), under exclusive licence to American College of Neuropsychopharmacology 2021

Methamphetamine (Meth) is a powerful illicit psychostimulant, widely used for recreational purposes. Besides disrupting the monoaminergic system and promoting oxidative brain damage, Meth also causes neuroinflammation, contributing to synaptic dysfunction and behavioral deficits. Aberrant activation of microglia, the largest myeloid cell population in the brain, is a common feature in neurological disorders triggered by neuroinflammation. In this study, we investigated the mechanisms underlying the aberrant activation of microglia elicited by Meth in the adult mouse brain. We found that binge Meth exposure caused microgliosis and disrupted risk assessment behavior (a feature that usually occurs in individuals who abuse Meth), both of which required astrocyte-to-microglia crosstalk. Mechanistically, Meth triggered a detrimental increase of glutamate exocytosis from astrocytes (in a process dependent on TNF production and calcium mobilization), promoting microglial expansion and reactivity. Ablating TNF production, or suppressing astrocytic calcium mobilization, prevented Meth-elicited microglia reactivity and re-established risk assessment behavior as tested by elevated plus maze (EPM). Overall, our data indicate that glial crosstalk is critical to relay alterations caused by acute Meth exposure.

Neuropsychopharmacology (2021) 46:2358–2370; <https://doi.org/10.1038/s41386-021-01139-7>

INTRODUCTION

Methamphetamine (Meth) is a potent and highly addictive psychostimulant that causes persistent harmful effects in the central nervous system (CNS) [1, 2]. While initial Meth use leads to long-lasting euphoria, high energy, hyperactivity, hypersexuality, and decreased anxiety, repeated exposure results in anxiety, sleep disturbances, insomnia, paranoia, cognitive dysfunction and memory impairment, which are associated with brain damage in frontostriatal and limbic regions, including higher risk of stroke [3]. At the molecular level, Meth toxicity is classically characterized by severe disruption of the dopaminergic system, causing high oxidative stress, neuronal dysfunction [4, 5], and increased release of proinflammatory mediators and glutamate [6, 7].

There is a growing understanding that the interplay between neuronal and glial cells is essential for developing and maintaining addiction [8–10]. Gliotransmission is implicated in drug-seeking modulation, with a particular focus on glutamatergic signaling [11, 12], that can trigger calcium influx, leading to reactive oxygen species (ROS) formation and subsequent oxidative damage [13]. However, the overall contribution of such mechanisms to the addictive process remains unclear [14, 15].

Microglia and astrocytes play crucial roles in brain injury and repair [16, 17]. Still, their sustained reactivity—often increasing

the production of proinflammatory mediators like tumor necrosis factor (TNF), glutamate, and ROS [18, 19]—may result in damage to the brain parenchyma [20, 21]. Upon exposure to psychoactive substances, microglia may also become highly reactive, augmenting the release of proinflammatory mediators [14]. Moreover, microglia reactivity increases the likelihood of relapse in early abstinence [10, 14]. Therefore, a better understanding of the role of microglia reactivity and associated brain immune-pathways in response to psychostimulants is paramount to implement relevant interventions for treating addictive behaviors. In accordance, we have demonstrated that binge alcohol administration to adult mice causes aberrant synaptic pruning and loss of prefrontal cortex excitatory synapses, increasing anxiety-like behavior, which is prevented by pharmacological blockade of Src activation or by reducing TNF production in microglia [22].

Here, we investigated how Meth interferes with microglia reactivity. Our results showed that the behavioral alterations caused by binge Meth exposure are mediated by astrocyte-microglia crosstalk in which release of glutamate from astrocytes in a TNF/IP₃ receptor (IP₃R)/SNARE-dependent manner leads to microglial activation, neuroinflammation, and ultimately to changes in mice behavior.

¹Addiction Biology Group, i3S-Instituto de Investigação e Inovação em Saúde and IBMC - Instituto de Biologia Molecular e Celular, Universidade do Porto, Porto, Portugal.

²Faculdade de Medicina da Universidade do Porto (FMUP), Porto, Portugal. ³Glial Cell Biology Group, i3S-Instituto de Investigação e Inovação em Saúde and IBMC - Instituto de Biologia Molecular e Celular, Universidade do Porto, Porto, Portugal.

⁴Instituto de Ciências Biomédicas de Abel Salazar (ICBAS), Universidade do Porto, Porto, Portugal. ⁵Life and Health Sciences Research Institute (ICVS), School of Medicine, University of Minho, Braga, Portugal.

⁶ICVS/3B's - PT Government Associate Laboratory, Braga/Guimarães, Portugal.

⁷IPCA-EST-2Ai, Polytechnic Institute of Cávado and Ave, Applied Artificial Intelligence, Barcelos, Portugal. ⁸ESS.PP, Escola Superior de Saúde do Politécnico do Porto, Porto, Portugal.

⁹These authors contributed equally: Teresa Canedo, Camila Cabral Portugal. ✉email: camila.portugal@ibmc.up.pt; tsummavi@ibmc.up.pt

Received: 30 March 2021 Revised: 12 July 2021 Accepted: 24 July 2021

Published online: 16 August 2021

MATERIALS AND METHODS

Animals

All experiments were conducted following the Directive 2010/63/EU and approved by the competent authorities Direção Geral de Alimentação e Veterinária (DGAV) and i3S Animal Ethical Committee (ref.2018-13-TS and DGAV ref.003891/2019-02-15). Researchers involved in animal experimentation were FELASA certified. All efforts were made to minimize animal suffering and the number of animals used.

Mice were housed under specific pathogen-free conditions, controlled environment (20 °C, 45–55% humidity) with an inverted 12 h/12 h light/dark cycle, and free access to food and water. Because of the potential behavioral variability related to the estrous cycle in females [23], only male mice were used. C57BL/6 male mice were obtained from the i3S animal facility. TNF knockout mice in the C57BL/6 background (referred herein as TNF KO) were kindly supplied by Professor Rui Appelberg (University of Porto). TNF KO mice [22] were maintained at i3S and genotyped by PCR using ATCCGCGACTGGAAGTGGCAGAA (forward) and CTGCCCGACTCCGCAAAGTCTAA (reverse) primer pair. IP₃R2 KO mice [24, 25] were housed at ICVS animal facility and genotyped by PCR using the primer pairs: WT (F, 5'-ACCCTGATGAGGGAAGTCT-3'; R, 5'-ATCGATTCATAGGGCA CACC-3') and mutant allele (neo-specific primer: F, 5'-AATGGGCTGAC CGTTCCTCGT-3'; R, 5'-TCTGAGAGTGCTGGCTTTT-3').

Mice drug treatment

Mice were treated using a Meth binge protocol [26, 27] and randomly assigned to the treated group (4 × 5 mg/kg Meth, 2 h apart, intraperitoneally) or the control group (4x isovolumetric saline), and sacrificed 24 h after the first administration as schematized in Supplementary Fig. 1A. Since Meth causes hyperthermia [28], we controlled body temperature through infrared readings every 20 min using subcutaneous tags (Biomark, ID, USA). Meth significantly increased body temperature (Supplementary Fig. 1B) but without exceeding critical values. Methamphetamine hydrochloride was imported from Sigma-Aldrich (MO, USA) under a special INFARMED license (ref. 290-13).

Fluorescence-activated cell sorting (FACS) and RNA extraction for sequencing

Twenty-four hours after the first Meth administration, animals were perfused under deep anesthesia with ice-cold PBS. The brains were removed and collected in ice-cold medium A (HBSS, Thermo Scientific MA, USA) supplemented with 15 mM HEPES and 0.6% glucose. Microglia were isolated from adult mice brains as previously described [29]. Microglia (CD11b⁺CD45^{low}CD206⁻) were sorted on the FACS ARIA (BD Immunocytometry Systems, CA, USA) using the following antibodies: CD45-PE (103106), CD11b-PE/Cy7 (101215), and CD206-APC (141707), obtained from BioLegend (CA, USA). Total RNA was isolated using the RNeasy Plus Micro Kit (Qiagen, Düsseldorf, DE) according to the manufacturer's instructions. RNA's integrity was analyzed using the Bioanalyzer 2100 RNA Pico chips (Agilent Technologies, CA, USA), according to manufacturer instructions.

Library preparation and sequencing

Ion Torrent sequencing libraries were prepared according to the AmpliSeq Library prep kit protocol. Briefly, 1 ng of highly intact total RNA was reverse transcribed, the resulting cDNA was amplified for 16 cycles by adding PCR Master Mix, and the AmpliSeq mouse transcriptome gene expression primer pool. Amplicons were digested with the proprietary FuPa enzyme, then barcoded adapters were ligated onto the target amplicons. The library amplicons were bound to magnetic beads, and residual reaction components were washed off. Libraries were amplified, re-purified, and individually quantified using Agilent TapeStation High Sensitivity tape. Individual libraries were diluted to a 50 pM concentration and pooled equally. Emulsion PCR, templating and 550 chip loading were performed with an Ion Chef Instrument (Thermo Scientific). Sequencing was performed on an Ion S5XL™ sequencer (Thermo Scientific). Bioinformatic analyses are detailed in the Supplementary Methods section.

Flow cytometry

Microglia and macrophages were analyzed, as we previously described [30, 31]. Briefly, mice were anesthetized and perfused with ice-cold PBS. The whole brain was quickly removed and mechanically homogenized. The cell suspension was passed through a 100 μm cell strainer and centrifuged over a discontinuous 70%/30% Percoll gradient. Cells on the interface were

collected, pelleted, and resuspended in FACS buffer (2% BSA; 0.1% Sodium Azide in PBS). Cells were counted using the Countess TM automated counter (Thermo Scientific). For microglia and macrophage characterization, the following antibodies were used: CD45-PE (103106), CD11b-AF647 (101218), Ly6C-PerCP/Cy5.5 (128012), CCR2-PE/Cy7 (150611), and MHCI-BV421 (107631), obtained from BioLegend. Samples were evaluated on FACS Canto II (BD Immunocytometry Systems).

Immunohistochemistry

Mice were anesthetized and perfused with ice-cold PBS, followed by 4% paraformaldehyde (PFA). Brains were post-fixed overnight, cryoprotected using sucrose gradient (15 and 30%), embedded in OCT, frozen, and cryosectioned (coronally at 30 μm, between Bregma positions 1.0 mm–2.0 mm) in the CM3050S cryostat (Leica Biosystems, Wetzlar, DE). Brain sections were collected on adherent slides and stored at –20 °C.

For immunolabeling, brain slides were defrosted and permeabilized with 0.25% Triton X-100 for 15 min. Then, brain sections were blocked with 3% BSA, 0.1% Triton X-100 and 5% FBS for 1 h. Primary antibodies were incubated overnight (4 °C) under the manufacturer's recommendations. After washing, sections were incubated with secondary antibodies conjugated to Alexa Fluor for 2 h (RT). After PBS washes, sections were mounted using Fluoroshield (Sigma-Aldrich) and visualized in a TCS SP5 II confocal microscope (Leica Biosystems). Antibodies are described in Supplementary Table 4.

Microglial morphometric analysis and CD68 in vivo immunolabeling

Coronal brain sections (30 μm) from the striatum and hippocampus were obtained using the CM3050S cryostat (Leica Biosystems). Brain sections were incubated (free floating) with blocking solution (10% horse serum, 0.2% Triton X-100 in PBS) for 1 h (RT). Primary antibodies (Supplementary Table 4) were incubated in blocking solution for 72 h (4 °C) with agitation. After several washes, secondary antibodies (Supplementary Table 4) were incubated for 24 h (4 °C) with agitation and nuclei were stained with DAPI. Images were acquired on a TCS SP5II resonant scanner confocal microscope (Leica Biosystems). Microglia 3D reconstructions were performed using the IMARIS software (version 9.6.1, Bitplane, Belfast, UK) for 13–17 cells/group from *n* = 3 mice per group.

Primary cultures

Primary mixed glial cultures were performed as previously described [30, 32]. Briefly, neonatal Wistar rats, C57BL/6 or TNF KO mice were sacrificed, and their cerebral cortices dissected and digested with 0.07% trypsin-EDTA in the presence of DNase for 15 min (37 °C). Cells were dissociated and seeded in poly-D-Lysine-coated T-flasks at 1.5 × 10⁶ cells/cm² in DMEM GlutaMAX™-I supplemented with 10% FBS, 1% Penicillin-Streptomycin. Culture media was changed every three days up to 21 days. All cultures were kept at 37 °C with 95% air/ 5% CO₂ in a humidified incubator.

To obtain purified microglia cultures, flasks were shaken (200 rpm, 2 h) to detach microglia. The culture media containing microglia were collected, centrifuged (453 g, 5 min), resuspended, and plated in glass coverslips at 2.5 × 10⁵ cells/cm² in DMEM-F12 GlutaMAX™-I supplemented with 10% FBS, 0.1% Penicillin-Streptomycin and 1 ng/ml GM-CSF. Purified microglia were cultured for 4–7 days. Immunolabeling with CD11b showed a purity of 95–99%.

For purified astrocytic cultures, mixed glial cell cultures were shaken (220 rpm, overnight) to remove non-astrocytic cells. Next, astrocytes (adherent cells) were detached and split into non-coated T-flasks in DMEM GlutaMAX™-I supplemented with 10% FBS and 1% Penicillin-Streptomycin. Split cultures were re-split at least four times to obtain purified cultures. After that, astrocytes were plated at 2.5 × 10⁴ cells/cm² in non-coated plates and maintained for 3–4 days.

Preparation of astrocyte-conditioned medium

After two days in culture, astrocytes were left untreated (control) or incubated with 100 μM Meth [33] for 24 h. Untreated astrocyte-conditioned medium (ACM CT) and conditioned medium from Meth-treated astrocytes (ACM Meth) were collected, centrifuged for debris removal (1200 rpm, 5 min), and frozen at –80 °C until used. To evaluate astrocytic conditioned media's effects, the culture media from purified microglial cell cultures were totally removed and cell were exposed to ACM CT or ACM Meth for 24 h.

Cell treatments

Microglia cells were treated with 100 μ M Meth (Sigma-Aldrich), 1 μ g/mL lipopolysaccharide (LPS, Sigma-Aldrich), 0.1 μ M–1 mM glutamate (Sigma-Aldrich), or 100 μ M (RS)- α -Cyclopropyl-4-phosphonophenylglycine (CPPG, Tocris, Bristol, UK). Astrocytes were treated with 100 μ M Meth (Sigma-Aldrich), 10 μ M BAPTA-AM, 500 nM XestospongineC (XeC, Tocris), 500 nM Tetanus toxin (tetX, Sigma-Aldrich), or 50 nM TNF (PeproTech, LND, UK).

Immunocytochemistry

Immunocytochemistry was performed as we previously described [30, 32]. Briefly, after fixation with 4% PFA, cultures were permeabilized with 0.1% Triton X-100 for 10 min and blocked with 3% BSA for 1 h. Next, cells were incubated with primary antibody under the manufacturer's recommendations, washed, and incubated with secondary antibodies conjugated with Alexa Fluor 488 or 568 for 1 h (RT). Finally, cells were incubated with DAPI, mounted, and visualized using a DMI6000B inverted microscope (Leica Microsystems) with an HCX Plan Apo 63x/1.3 NA glycerol immersion objective. Images were acquired with 2x2 binning using a digital CMOS camera (ORCA-Flash4.0 V2, Hamamatsu Photonics, Hamamatsu, JPN). Antibodies are described in Supplementary Table 5.

Phagocytic assay

The phagocytic assay was performed as previously described [34, 35]. Briefly, fluorescent latex beads (Sigma-Aldrich) were diluted in culture medium (0.001%) and incubated for 1 h. After that, cells were washed and fixed with 4% PFA. Immunocytochemistry for CD11b was performed, and the phagocytic efficiency of microglia was estimated as we did before [34].

Reactive oxygen species (ROS)

Primary microglia cultures were incubated with CellROX[®] green reagent (Thermo-Fisher Scientific), according to the manufacturer's recommendations. Cells were observed using a DMI6000B inverted microscope (Leica Microsystems) with an HCX Plan Apo 63x/1.3 NA glycerol immersion objective. Images were acquired with 4 × 4 binning using a digital CMOS camera (ORCA-Flash4.0 V2, Hamamatsu Photonics).

Fluorescence quantification and colocalization analysis

For the intensity quantification, images were exported using the Leica LAS AF program in TIFF format (16-bit). Background subtraction, image segmentation, and determination of the intensity of the fluorescence signals were processed in Fiji software as before [30]. Automated fluorescence imaging and quantification in primary microglial cells seeded in 96-well plates (data from Fig. 3E and F) was further detailed in Supplementary Methods section. For colocalization analyses, images were acquired using an HCX Plan Apo 63x/1.4–0.6 NA oil immersion objective in 16-bit sequential mode using bidirectional TCS mode at 100 Hz with the pinhole kept at one airy in the Leica TCS SP5 II confocal microscope (Leica Microsystems). The Coloc2 plug-in in Fiji was used to establish TNF/GFAP channels' quantitative colocalization as we did before [32].

RNA extraction, cDNA synthesis, and qRT-PCR

Total RNA was isolated from hippocampus and striatum tissue using the PureLink[®] RNA Mini-Kit (Thermo-Fisher Scientific) according to the manufacturer's specifications. RNA from cell cultures was isolated using the RNeasy Mini-Kit (Qiagen). cDNA synthesis was performed using 1 μ g of total RNA using RT2 Easy First Strand Kit (Qiagen). qRT-PCR was performed using iQ[™] SYBR[®] Green Supermix on an iQ[™]5 multicolor real-time PCR detection system (Bio-Rad, CA, USA). All primers (Sigma-Aldrich) are described in Supplementary Table 6. Raw data were analyzed using the 2^{- Δ CT} method with Yhwaz or S18 serving as internal control genes in cell cultures or brain tissue, respectively. Results were expressed in relative gene abundance.

FRET assays

Primary microglia or astrocytes were plated on plastic-bottom culture dishes μ -Dish35mm (iBidi, Martinsried, DE) and transfected with FRET biosensor for glutamate (pDisplay FLIPE-600n, plasmid 13545), ROS (pFRET-HSP33 cys, plasmid 16076) or calcium (pcDNA-D1ER, plasmid 36325), all from Addgene (MA, USA) using jetPRIME[®] (Polyplus, NY, USA). Imaging was performed using a Leica DMI6000B inverted microscope, and images were processed in Fiji software exactly as before [36].

Enzyme-linked immunosorbent assay (ELISA)

ELISA was used to quantify the concentration of glutamate present in ACM CT and ACM Meth following the instructions provided by the manufacturer (ImmuSmol, Bordeaux, FR). Absorbance at 450 nm, with wavelength correction at 620 nm, was measured with a multimode microplate reader (Synergy HT, Biotek, USA). Values corresponding to glutamate in μ M were obtained by interpolating a standard curve using increasing glutamate concentrations (μ M).

Elevated plus-maze (EPM)

Anxiety-like behavior was assessed using the elevated plus maze (EPM) test as we previously described [22, 37]. The test was performed 24 h after the first Meth administration, just before the euthanasia. The test was conducted in the dark phase of the light/dark cycle. The mice's movement and location were analyzed by an automated tracking system equipped with an infrared-sensitive camera (Smart Video Tracking Software v 2.5, Panlab, Harvard Apparatus). The maze, made of opaque gray polyvinyl, consisted of four arms arranged in a cross-shape; two closed arms have surrounding walls (18 cm high), opposing two open arms (all arms 37 × 6 cm). The apparatus was elevated at the height of 50 cm. Each mouse was placed on the central platform facing an open arm and allowed to explore the maze for 5 min.

Statistical analysis

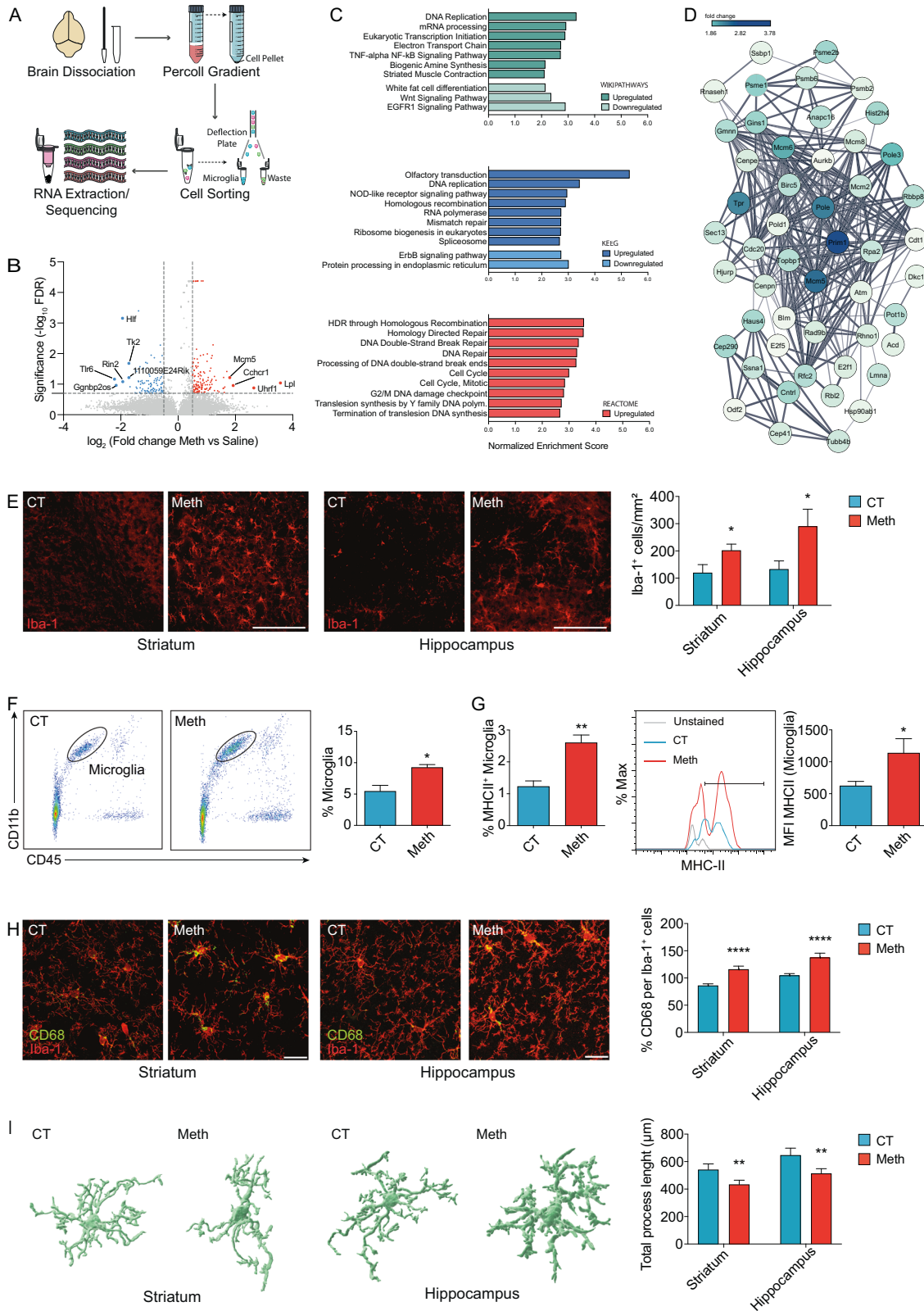
A 95% confidence interval was used, and statistical significance was set at $P < 0.05$. Results were expressed as mean \pm SEM (standard error of the mean). Gene clusters were compared by contingency analysis using Fisher's exact test and the Baptista-Pike method to calculate the odds ratio. Experimental units in individual replicates were evaluated for Gaussian distribution using the D' & Pearson omnibus normality test. When comparing only two experimental groups, the unpaired Student *t* test with equal variance assumption was used for data with normal distribution, and the Mann-Whitney test was used otherwise. When comparing three or more groups, a one-way analysis of variance (ANOVA), followed by the Bonferroni or Tukey post hoc test was used for data with normal distribution, the Kruskal-Wallis test followed by Dunn's multiple comparisons was used otherwise. To compare different groups with two independent variables, we used a two-way ANOVA followed by the two-stage linear step-up procedure of Benjamini, Krieger, and Yekutieli. All quantifications were performed blinded. Analysis were performed using the GraphPad Prism[®] software version 9.1.2. for macOS.

RESULTS

Microglia exposed to Meth display a core cell cycle-related transcriptomic signature

To clarify the action of Meth in microglia, we used a binge pattern of Meth administration in adult mice (Supplementary Fig. 1A) and conducted RNA-Seq analysis in flow cytometry-sorted microglia (CD11b⁺ CD45^{low} CD206⁻) from whole-brain tissue (Fig. 1A). Out of the 23,930 microglial transcripts identified, 207 were significantly altered after binge Meth administration (Fig. 1B, Supplementary Tables 1 and 2). To pinpoint the most relevant biological pathways altered in the microglial transcriptome after Meth exposure, we performed gene set enriched analysis (GSEA). GSEA using Wikipathways, KEGG, and REACTOME databases revealed a prominent upregulation of cell cycle-related pathways (including DNA Replication, Eukaryotic Transcription Initiation, Homologous recombination, Mismatch repair, DNA Repair, DNA Double-Strand Break, G2/M DNA damage checkpoint, Mitotic Cell Cycle, Cell Cycle) (Fig. 1C and detailed data in Supplementary Table 3), possibly associated with Meth-induced microglial expansion. Of note, the TNF-alpha NF-kB and the NOD-like receptor signaling pathways, both related to proinflammatory signaling, were also upregulated (Fig. 1C).

The combined cell cycle-related transcriptomic cluster (the top 50 upregulated transcripts are displayed as a network in Fig. 1D) contained as highest altered transcripts the DNA primase small subunit (Prim1), the DNA polymerase epsilon catalytic subunit A (Pole), the DNA polymerase epsilon subunit 3 (Pole3), the translocated promoter region, nuclear basket protein (Tpr), and



the DNA helicases MCM5 and MCM6 (Fig. 1D). Thus, initiation of DNA replication, DNA mismatch repair, homologous recombination, and telomere C-strand synthesis (licensed by the epsilon DNA polymerase complex and the MCM complex via 3'-5' exodeoxyribonuclease and 3'-5' DNA helicase activities) are plausibly the

most strongly affected microglial pathways following Meth exposure.

Next, we compared our cluster of 207 differentially expressed transcripts upon Meth exposure with clusters previously reported for the microglial signature program [38, 39], aging [40],

Fig. 1 Meth triggers microglial activation in the brain. **A** Schematic representation of conducted workflow of microglial cell sorting and sequencing. **B** Volcano plot depicting differentially expressed genes of isolated microglia from brains of mice administered with binge Meth vs Saline ($n = 3$ mice per group). Non-differentially expressed genes are shown with gray dots, red dots represent significantly upregulated genes and blue dots represent downregulated genes. **C** Top 10 enriched pathways revealed by WikiPathways, KEGG and Reactome databases using Gene Set Enrichment Analysis (GSEA). **D** A network analysis of enriched gene sets involved in the cell cycle. The network represents the top 50 upregulated genes related to cell cycle, upon Meth treatment. **E** Representative confocal imaging of striatal and hippocampal sections from mice administered with binge Meth or saline (CT) and immunostained for Iba1. Graph displays (mean and SEM) the number of Iba1⁺ cells per area (3–4 sections/animal from $n = 3$ mice per group). * $p < 0.05$, two-way ANOVA showing only a significant effect for treatment, followed by the two-stage linear step-up procedure of Benjamini, Krieger and Yekutieli. Scale bars 50 μm . **F** Flow cytometry analyses of microglia cells (CD11b⁺CD45^{low}) isolated from the brains of mice administered with binge Meth or saline (CT) ($n = 5$ mice per group). The graph displays (mean and SEM) the percentage of microglial cells. * $p < 0.05$ (unpaired t test). **G** Expression of MHCII by flow cytometry in microglia (CD11b⁺CD45^{low}) isolated from the brains of mice administered with binge Meth or saline (CT) ($n = 5$ mice per group). Graphs display (means and SEM) the percentage of microglial cells expressing the MHCII marker and the mean fluorescence intensity (MFI) of MHCII in microglial cells. * $p < 0.05$, *** $p < 0.01$ (unpaired t test). **H** Representative confocal imaging of striatal and hippocampal sections from mice administered with binge Meth or saline (CT) and immunostained for Iba1 (red) and CD68 (green). Graph displays (mean and SEM) the percentage of CD68 expression per Iba1⁺ cells (at least 30 cells were quantified from each animal; $n = 3$ mice per group). **** $p < 0.0001$ (CT vs Meth), two-way ANOVA (treatment \times region) revealed also a significant effect of the region ($p < 0.001$). The two-stage linear step-up procedure of Benjamini, Krieger, and Yekutieli was used as a pos-hoc. Scale bars 20 μm . **I** Imaris (Bitplane)-based three-dimensional reconstructions of representative microglia from striatal and hippocampal sections obtained from mice administered with binge Meth or saline (CT). Graph displays (mean and SEM) of Imaris-based automated quantification of microglial total process length (13–17 cells/group from $n = 3$ mice per group). ** $p < 0.01$ (CT vs Meth), two-way ANOVA (treatment \times region) revealed also a significant effect for the region ($p < 0.05$). The two-stage linear step-up procedure of Benjamini, Krieger, and Yekutieli was used as a pos-hoc.

disease-associated (DAM) [41], injury-related (IRM) [40], drug exposure [42, 43], or the microglial engulfment module [38] (Supplementary Fig. 1C and Table 7). Interestingly, we only found a positive association of the Meth-induced cluster with the aging clusters. These data indicate that Meth exposure does not affect the classical signature programs of healthy or diseased microglia but are in line with reports showing that Meth might foster cellular and tissue aging [44].

Meth activates microglia in vivo

Instructed by the RNA-Seq data, which showed a marked upregulation of cell cycle-related pathways, we evaluated the effect of Meth on microglial expansion. The increase in expression of cell cycle-related transcripts correlated with a significant expansion in the number of Iba1⁺ cells on tissue sections obtained from the striatum and the hippocampus (Fig. 1E) of mice exposed to Meth when compared to saline-treated (control) mice. This increase in microglial numbers was further confirmed by flow cytometry in whole-brain tissue (Fig. 1F and Supplementary Fig. 2A for gating strategy). We also analyzed the brain macrophage population (CD11b⁺CD45^{high}) and found no differences between Meth-treated and control mice in total, Ly6C⁺, or Ly6C⁺CCR2⁺ macrophages (Supplementary Fig. 2A). Because the RNA-Seq also showed Meth-induced alterations in microglial proinflammatory signaling, we evaluated the levels of MHCII, a classical microglial proinflammatory marker. We found an increase in the percentage of microglial cells expressing MHCII and an increase in the expression of MHCII in microglia from Meth exposed mice (Fig. 1G). We also evaluated changes in the expression of CD68, a lysosomal protein highly expressed in activated microglia. We found increased CD68 staining within microglia from the striatum and hippocampus (Fig. 1H).

To better characterize microglia activation, we analyzed several morphologic parameters in striatal and hippocampal microglia. Our results evidenced Meth-induced reduction in microglial total process length (Fig. 1I) and number of branching points, as well as reduced territorial area and territorial volume (Supplementary Fig. 2B). Sholl analysis confirmed such effect on microglial complexity (Supplementary Fig. 2C). In addition, we found a region effect (two-way ANOVA, showing significant region effect for CD68 expression $p < 0.001$, total process length $p < 0.05$, branching points $p < 0.001$, and territorial volume $p < 0.05$), which consistently showed that although microglial morphology differed between the striatum and the hippocampus, the degree of morphological alterations elicited by Meth

was overtly similar in the microglia from these regions (Fig. 1I and Supplementary Fig. 2B). Together, these results indicate that binge Meth administration increases microglial numbers and activation.

Meth activates microglia in an astrocyte dependent-manner

Because Meth activated microglia in vivo, we used an in vitro approach to dissect the microglial response to Meth. Using primary microglial cultures, we found that Meth (100 μM) diminished microglial capacity to phagocyte inert fluorescent beads (Fig. 2A) and did not increase the formation of ROS (Fig. 2B) nor the expression of iNOS (Fig. 2C). We also observed no differences in the mRNA transcript abundance of the proinflammatory cytokines IL-1 β , IL-6, and TNF compared to untreated microglia (CT, Fig. 2D). To further confirm that our microglial cultures were responsive to a classic proinflammatory stimulus, but not to Meth, we treated them with LPS (1 $\mu\text{g}/\text{mL}$). As expected, increased ROS formation and iNOS expression were observed in response to LPS (Supplementary Fig. 3A, B). We also analyzed classic microglial anti-inflammatory markers and found no significant alterations in arginase 1 expression (Fig. 2E) nor in the amounts of mRNA transcripts for IL-10 and TGF β (Fig. 2F). Here, we concluded that Meth does not activate microglia in a cell-autonomous manner. Thus, the transcriptomic changes observed in the RNA-Seq and the microgliosis observed in vivo might result from the collective crosstalk between microglia and other cell types.

Because astrocyte-derived signaling is essential in microglial activation [45], we tested the hypothesis that astrocytes could mediate Meth-induced microglia activation. To do that, we exposed primary microglia to conditioned media (CM) obtained from primary astrocytes treated with Meth (ACM Meth) or CM from control astrocyte cultures (ACM CT). Neither Meth nor ACM Meth affected astrocytic or microglial viability (Supplementary Fig. 3C). Using the CellRox[®] green reagent, we found an increase in ROS production in primary microglia exposed to ACM Meth compared with cultures exposed to ACM CT (Fig. 2G). To confirm the CellRox[®] effect, we used the HSP FRET biosensor [46]. We observed a consistent and fast increase (within 5 min) of ROS generation in living primary microglia exposed to ACM Meth (Supplementary Fig. 4A). Besides, primary microglia treated with ACM Meth displayed higher mRNA levels of the proinflammatory markers iNOS, IL-1 β , and IL-6, but not TNF (Fig. 2H). Primary microglia exposed to ACM Meth also displayed enhanced iNOS expression compared with cultures incubated with ACM CT

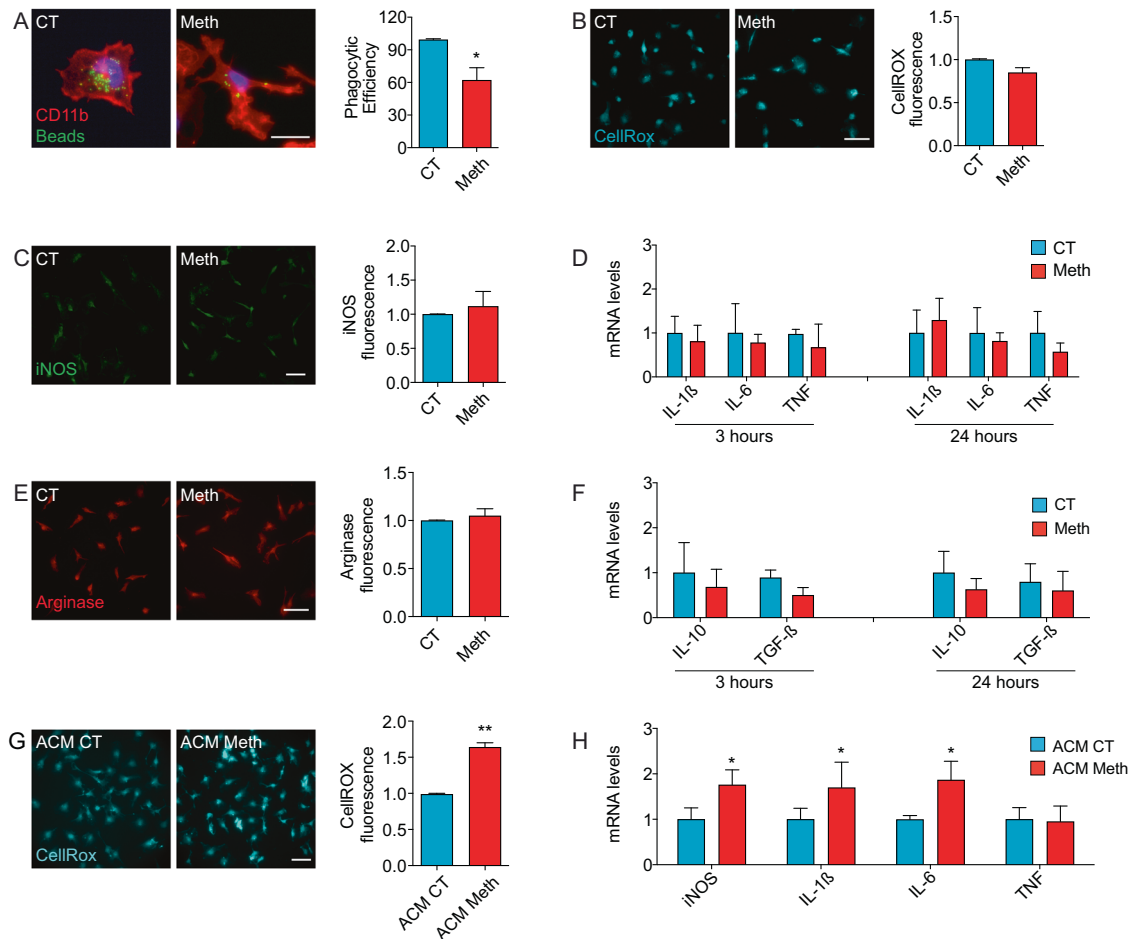


Fig. 2 Microglia activation triggered by Meth requires Astrocytes. **A** Fluorescence imaging of CD11b (red) in primary microglia incubated with microbeads (green) and treated with 100 μ M Meth for 24 h ($n = 3$ independent cultures). Graph (means and SEM) displays phagocytic efficiency. * $p < 0.05$ (unpaired t test). Scale bar 10 μ m. **B** Fluorescence imaging of primary microglia incubated with the CellROX[®] green reagent and treated with 100 μ M Meth for 24 h ($n = 3$ independent cultures). Graph (means and SEM) displays the CellROX[®] intensity normalized to the control values (unpaired t test). Scale bar 10 μ m. **C** Fluorescence imaging of primary microglia immunolabeled for iNOS (green) treated with 100 μ M Meth for 24 h ($n = 3$ independent cultures). Graph (means and SEM) displays iNOS intensity normalized to the control values (unpaired t test). Scale bar 10 μ m. **D** qRT-PCR for IL-1 β , IL-6, or TNF from primary microglia treated with 100 μ M Meth for 3 h or 24 h ($n = 3$ independent cultures). Graphs (means and SEM) display the indicated transcripts' mRNA expression levels (unpaired t test). **E** Fluorescence imaging of arginase in primary microglia treated with 100 μ M Meth for 24 h ($n = 3$ independent cultures). Graph (means and SEM) displays arginase intensity normalized to the control values (unpaired t test). Scale bar 10 μ m. **F** qRT-PCR for IL-10 or TGF β from primary microglia treated with 100 μ M Meth for 3 h or 24 h ($n = 3$ independent cultures). Graphs (means and SEM) display the indicated transcripts' mRNA expression levels (unpaired t test). **G** Fluorescence imaging of primary microglia exposed to conditioned media obtained from primary astrocytes treated with 100 μ M Meth (ACM Meth) or not (ACM CT) for 24 h and incubated with CellROX[®] green reagent ($n = 3$ independent cultures). Graph (means and SEM) displays the CellROX[®] intensity normalized to the ACM CT values ** $p < 0.01$ (unpaired t test). Scale bar 10 μ m. **H** qRT-PCR for iNOS, IL-1 β , IL-6, or TNF from primary microglia exposed to ACM CT or ACM Meth for 24 h ($n = 3-5$ independent cultures). Graphs (means and SEM) display the mRNA levels for the indicated transcripts. * $p < 0.05$ (unpaired t test).

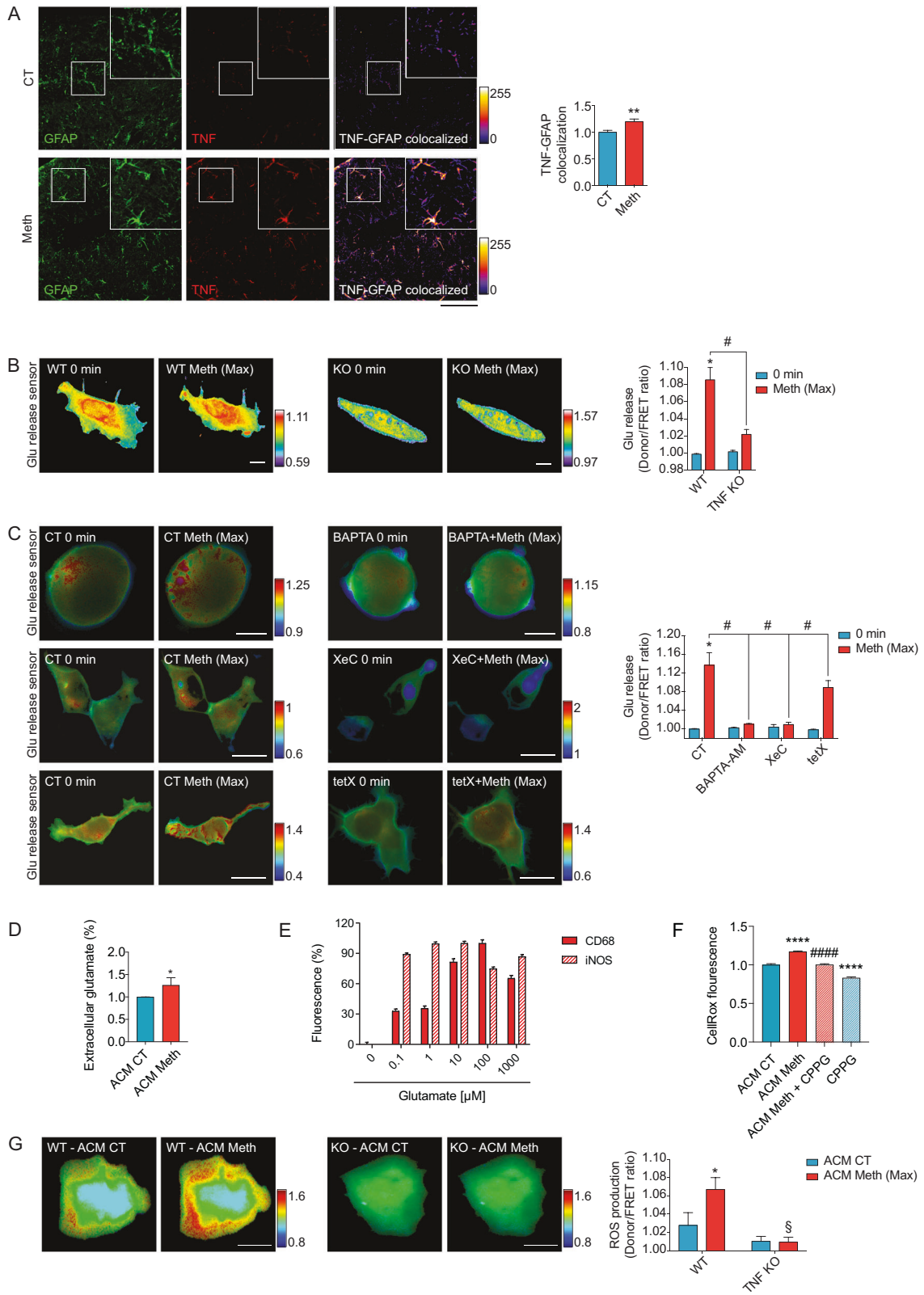
(Supplementary Fig. 4B). Thus, we concluded that upon Meth exposure, astrocytes could induce microglial activation.

Meth causes glutamate release via TNF and IP₃-dependent Ca²⁺ mobilization in astrocytes

Our RNA-Seq data revealed a Meth-induced enrichment of gene transcripts associated with the TNF- α NF- κ B Signaling Pathway (Fig. 1C). However, TNF expression was not increased in microglia (Supplementary Table 1 and 3 and Fig. 2D), including in response to ACM Meth (Fig. 2H). Because we observed an increase in TNF transcripts in specific brain regions following Meth exposure (Supplementary Fig. 3D), and in line with previous reports [47], we hypothesized that astrocytes were increasing TNF production in response to Meth. Accordingly, we observed by double-labeling immunofluorescence an increase in TNF content in astrocytes (GFAP⁺ cells) in the hippocampus of mice exposed to Meth

(Fig. 3A). The secretion of high amounts of TNF activates TNF receptor 1 (TNFR1) and leads to a substantial release of glutamate from primary astrocytes [48]. In agreement, using the glutamate-release FRET biosensor FLIPE600n^{SURFACE} [49], we found that TNF promoted a fast and sustained release of glutamate from living astrocytes (Supplementary Fig. 4C). Meth also caused robust glutamate release in primary astrocytes from WT mice, an effect not observed in primary astrocytes from TNF-deficient mice, thereby confirming that autocrine TNF signaling plays a crucial role in Meth-induced glutamate release from astrocytes (Fig. 3B, Supplementary Fig. 4D and Supplementary Video 1 and 2).

Astrocytes can release glutamate from intracellular pools through various mechanisms, including Ca²⁺-dependent and -independent pathways [50]. To test whether glutamate release from astrocytes under Meth exposure is Ca²⁺-dependent, we chelated cytosolic Ca²⁺ with BAPTA-AM (10 μ M) and observed an



inhibition of Meth-induced glutamate release (Fig. 3C and Supplementary Fig. 4E), suggesting that elevation of cytosolic Ca^{2+} is necessary for Meth-triggered astrocytic glutamate release.

The rise in cytosolic Ca^{2+} required for glutamate release from astrocytes may originate from the endoplasmic reticulum (ER)

through the Ca^{2+} -release channel inositol triphosphate receptor (IP_3R) [51]. Using the D1ER FRET biosensor [52], which detects the efflux of Ca^{2+} from the ER into the cytosol, we monitored the mobilization of Ca^{2+} in living astrocytes exposed to Meth or TNF (Supplementary Fig. 4F). Treatment of primary astrocytes with

Fig. 3 Meth activates microglia via astrocytic TNF production. **A** Confocal imaging of hippocampal sections from mice treated with Meth or saline (CT) and immunostained for GFAP (green) and TNF (red). Graph displays (means and SEM) the GFAP/TNF colocalization puncta normalized to the CT values (3–4 sections *per* animal from $n = 3$ mice *per* group). $**p < 0.01$ (unpaired *t* test). Scale bar 50 μm . **B** Primary astrocytes from WT or TNF KO mice expressing the glutamate release FRET biosensor (FLIPE) were exposed to Meth 100 μM . Time-lapses of CFP/FRET ratio changes for the FLIPE biosensor (normalized at 0 min) show the maximum effect of Meth in both genotypes and are coded according to the scale ($n = 3$ –8 cells pooled across 2–3 independent experiments). $*p < 0.05$ (two-way ANOVA vs WT 0 min); $\#p < 0.05$ (two-way ANOVA vs WT Meth). Scale bars 10 μm . **C** Primary astrocytes expressing the glutamate release FRET biosensor (FLIPE) were exposed to Meth, BAPTA-AM (10 μM) + Meth 100 μM (upper panels), Xestosponginc (XeC; 500 nM) + Meth 100 μM (middle panels) or Tetanus toxin (Tet; 500 nM) + Meth (bottom panels). Time-lapses of CFP/FRET ratio changes for the FLIPE biosensor (normalized at 0 min) show the maximum effect of Meth and are coded according to the scale ($n = 5$ –7 cells pooled across 3 independent experiments). $*p < 0.05$ (two-way ANOVA vs WT 0 min); $\#p < 0.05$ (two-way ANOVA vs WT Meth). Scale bars 10 μm . **D** Glutamate concentration in the culture supernatant from CT astrocytes (ACM CT) or treated with Meth for 24 h (ACM Meth) was quantified by ELISA. Graph displays (means and SEM) of glutamate concentration, normalized to control values ($n = 4$ independent cultures). The concentration of glutamate on ACM CT was $18.05 \pm 2.23 \mu\text{M}$. **E** Primary microglia cells were treated with a range of glutamate concentrations (0.1 μM , 1 μM , 10 μM , 100 μM , and 1 mM). Graph displays (means and SEM) for CD68 and iNOS intensity normalized to untreated cells (0.0 μM). One-way ANOVA revealed a significant effect of glutamate concentration: $p < 0.0001$ for CD68 intensity and $p < 0.0001$ for iNOS intensity. **F** Primary microglia cells were treated with ACM CT, ACM Meth alone or pre-treated with 100 μM of (RS)- α -Cyclopropyl-4-phosphonophenylglycine (CPPG, 30 min before ACM Meth) and CPPG alone (100 μM). Evaluations were conducted at 24 h of exposure ($n = 2$ independent cultures). Graph displays (means and SEM) ROS production (CellRox) normalized to ACM CT. $****p < 0.0001$ (vs ACM CT), $****p < 0.0001$ (vs ACM Meth) One-way ANOVA and Tukey pos-hoc. **G** Primary microglia from WT or TNF KO mice expressing the ROS FRET biosensor HSP were incubated with ACM CT and then exposed to ACM Meth 100 μM . Time-lapses of CFP/FRET ratio changes for the HSP biosensor (normalized at 0 min) show the maximum effect of Meth and are coded according to the scale ($n = 4$ cells pooled across two independent experiments). $*p < 0.05$, § non-significant. Scale bars 10 μm .

Meth (Supplementary Fig. 4F, blue circles) or TNF (Supplementary Fig. 4F red circles) triggered a fast and sustained decrease in the FRET/CFP ratio of the D1ER biosensor, indicating that both Meth and TNF promoted the mobilization of Ca^{2+} from the ER to the cytosol. To investigate the role of IP_3R in Meth-induced Ca^{2+} -mobilization, we used Xestosponginc C (XeC, 500 nM), an IP_3R antagonist [53]. We observed that XeC abolished glutamate release in living primary astrocyte cultures exposed to Meth (Fig. 3C and Supplementary Fig. 4E) or TNF (Supplementary Fig. 4G) and concluded that IP_3R -dependent Ca^{2+} mobilization is involved in Meth-induced glutamate release.

To test whether, in Meth-treated astrocytes, glutamate was released through an exocytic mechanism [54], we used the tetanus toxin (500 nM) to prevent Ca^{2+} -dependent assembling of the dnSNARE complex and the fusion of exocytic vesicles with the membrane [55]. We observed a significant attenuation in the Meth-induced CFP/FRET ratio change of the FLIPE biosensor (Fig. 3C and Supplementary Fig. 4E), indicating that, in astrocytes, Meth stimulates the exocytosis of glutamate-containing vesicles in a Ca^{2+} -dependent manner.

Because TNF controls astrocytic glutamate release, we hypothesized that TNF/glutamate signaling might be directly involved in microglia activation by astrocytes exposed to Meth. To test this hypothesis, we measured glutamate in the ACM and observed increased glutamate content in ACM Meth compared to ACM CT (Fig. 3D). To confirm that increasing the extracellular amounts of glutamate leads to microglial activation, we treated primary microglia with different glutamate concentrations (from 0.1 μM to 1 mM) and evaluated iNOS and CD68 expression. We found that glutamate concentrations of 0.1 μM or higher were sufficient to increase iNOS or CD68 expression (Fig. 3E), which confirms that Meth-induced increase in extracellular glutamate, including those in the range observed in the ACM (Fig. 3D), leads to microglial activation. To further show that microglial activation induced by ACM Meth depended on glutamate, we used the group II/III metabotropic glutamate receptor antagonist CPPG in microglia. We found that CPPG treatment blocked the microglial activation (here evaluated by ROS production) induced by ACM Meth (Fig. 3F).

Moreover, whereas the CM obtained from WT astrocytes exposed to Meth promoted ROS generation in primary microglia (Fig. 3G and Supplementary Fig. 4H), the CM obtained from TNF-deficient astrocytes exposed to Meth failed to increase microglial ROS production (Fig. 3G and Supplementary Fig. 4H). Thus, we

concluded that TNF/glutamate signaling is necessary to induce microglial activation by astrocytes.

Microglia activation requires TNF and IP_3R -dependent Ca^{2+} mobilization

Because Meth activates microglia via TNF-to- IP_3R signaling in astrocytes, we evaluated whether Meth-induced microgliosis required this signaling *in vivo*. Knowing that the IP_3R isoform 2 is the primary IP_3 receptor in astrocytes and the major source of Ca^{2+} -translocation from the ER into the cytosol in these cells [56], we challenged $\text{IP}_3\text{R}2$ KO and TNF KO mice with binge Meth administration (Supplementary Fig. 1A). We observed that the Meth-induced microgliosis in the striatum and the hippocampus was prevented in both KO mice compared to WT (Fig. 4A). Consistent with these findings, flow cytometry showed that the Meth-induced increase in the microglial population was also prevented in TNF and $\text{IP}_3\text{R}2$ KO mice (Fig. 4B).

Excessive glutamate and microglia overactivation can negatively affect behavior [57]. Since Meth-induced TNF production led to glutamate release from astrocytes in an IP_3R -dependent manner and activated microglia, we hypothesized that blocking TNF or IP_3R signaling could also affect the behavioral alterations elicited by Meth. Because microglia activation seems to be related with changes in anxiety [58], which is also affected by Meth use, we tested WT, $\text{IP}_3\text{R}2$ KO and TNF KO mice in the EPM. We found that WT mice exposed to Meth displayed increased time and distance traveled in the open arms (Fig. 4C) and decreased the frequency of stretch-attended postures, protected head dipping (Supplementary Fig. 5A, B), while the total traveled distance was lower than for the control saline group (Fig. 4C). The latency to enter open arms is also shown in Supplementary Fig. 5C. Such behavioral pattern in the EPM, which is consistent with reduced anxiety-like behavior and decreased risk assessment, was significantly attenuated in TNF or $\text{IP}_3\text{R}2$ KO mice (Fig. 4C). These *in vivo* data confirm the relevance of the TNF/ Ca^{2+} mobilization-signaling for Meth-induced microglia activation.

DISCUSSION

Although Meth induces a microglia proinflammatory response *in vivo* [26, 59], the mechanisms involved in this process are still poorly understood. Herein, we found that Meth-induced microglia reactivity requires a crosstalk with astrocytes, mediated by glutamate release in a TNF- and $\text{IP}_3\text{R}/\text{Ca}^{2+}$ -dependent manner

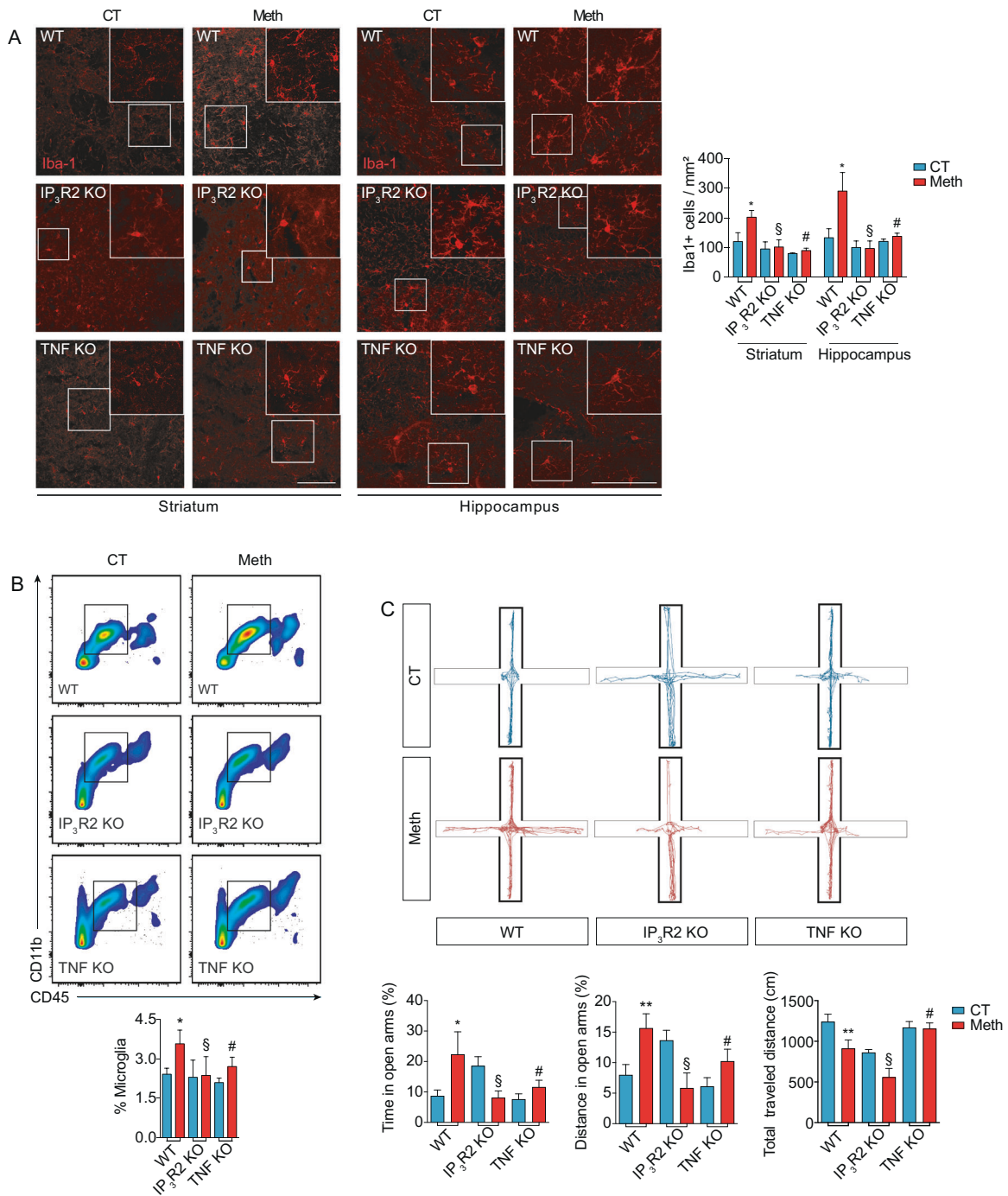


Fig. 4 TNF or IP₃R2 deficiency prevents Meth-induced microgliosis and behavioral changes. **A** Confocal imaging of striatal and hippocampal sections from WT, IP₃R2 KO, or TNF KO mice administered with binge Meth or saline (3–4 sections/animal from *n* = 3 mice *per* group) and immunostained for Iba1. Graph (means and SEM) displays the number of Iba1⁺ cells **p* < 0.05 WT-CT vs. WT-Meth; [§]non-significant (IP₃R2 KO-CT vs. IP₃R2 KO-Meth and [#]non-significant TNF KO-CT vs. TNF KO-Meth). Two-way ANOVA followed by the two-stage linear step-up procedure of Benjamini, Krieger and Yekutieli. Scale bars 50 μm. **B** Flow cytometry analysis of microglia cells (CD11b⁺CD45^{low}) isolated from WT, IP₃R2 KO, or TNF KO mice administered with Meth or saline (CT) (*n* = 5–9 animals *per* group). The graph displays the percentage of microglia cells with mean and SEM. **p* < 0.05 WT-CT vs. WT-Meth; [§]non-significant IP₃R2 KO-CT vs. IP₃R2 KO-Meth and [#]non-significant TNF KO-CT vs. TNF KO-Meth. Two-way ANOVA followed by the two-stage linear step-up procedure of Benjamini, Krieger and Yekutieli. **C** WT, IP₃R2 KO, and TNF KO animals were evaluated in the EPM 24 h after a binge pattern of Meth or saline (CT) administration (*n* = 6–13 animals *per* group). Graphs display (means and SEM) CT and Meth-treated mice displayed significant differences in time spent in open arms (OA), distance traveled in OA and in total traveled distance. **p* < 0.05 or ***p* < 0.01, WT-CT vs. WT-Meth; [§]non-significant IP₃R2 KO-CT vs. IP₃R2 KO-Meth and [#]non-significant TNF KO-CT vs. TNF KO-Meth. Two-way ANOVA followed by the two-stage linear step-up procedure of Benjamini, Krieger, and Yekutieli.

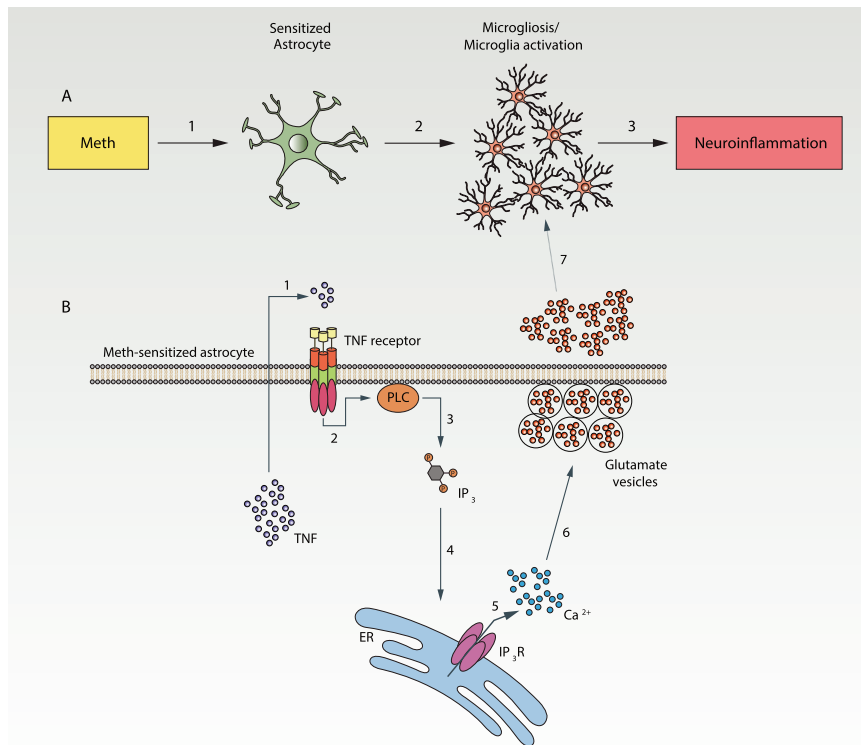


Fig. 5 Meth-induced microglia activation occurs via astrocytes. A Exposure to Meth induces astrocytic sensitization (1). Meth-sensitized astrocytes secrete soluble factors (2) that will act on microglia causing microgliosis and microglia activation, promoting neuroinflammation (3). **B** In Meth-sensitized astrocytes, Meth exposure triggers the production and secretion of TNF (1). TNF acts on astrocytic TNF receptors in an autocrine manner, leading to the activation of PLC (2). TNF-induced PLC activation produces the second messenger IP₃ (3) that interacts with IP₃ receptors on the ER (4). Activation of IP₃R promotes Ca²⁺-mobilization from the ER into the cytosol (5), consequently increasing glutamate release (6). Increased glutamate and TNF content in the extracellular milieu promotes the activation of microglia (7). Although our work focuses on the TNF-dependent effect on glutamate release, TNF released from astrocytes can interact with TNFRs present in the microglia and contribute to microglial activation observed in response to Meth. TNF tumor necrosis factor, PLC Phospholipase C, IP₃ Inositol (1,3,4) phosphate, ER endoplasmic reticulum, Ca²⁺ calcium ions, TNFR tumor necrosis factor receptor.

and that blocking IP₃R or TNF signaling prevented microglia activation elicited by Meth.

Consistently with previous findings [60, 61], our study shows that binge Meth caused microglial expansion, altered microglial morphology and increased the expression of proinflammatory markers that are hallmarks of many neurodegenerative diseases [62]. The range of enriched pathways related to cell cycle modulation associated with the microglial expansion confirmed the relevance of this Meth-induced effect. Astrocytic glutamate, likely in combination with TNF, is potentially involved in the proliferative effect of Meth on the microglia. The top upregulated cell cycle-related transcripts (revealed by the RNA-Seq) induced by Meth in microglia (Prim1, Pole, Pole3, MCM5, and MCM6) share a specific transcriptional regulatory program controlled by the transcription factor activating protein-1 (AP-1), whose activity strongly rely on cAMP and calcium signaling triggered by neurotransmitters and cytokines. Indeed, increasing the cytosolic levels of cAMP or calcium is one of the first signaling events elicited by exogenous glutamate (via activation of glutamate metabotropic receptors) or TNF (via the activity of TNFR1) that trigger AP-1-dependent transcriptional activation. Thus, triggering of AP-1-dependent transcription by glutamate/TNF signaling is likely involved in the mitogenic effect elicited by Meth in hippocampal and striatal microglia.

To characterize the molecular mechanisms involved in Meth-induced microglia activation, we analyzed Meth effects directly on

purified microglia cultures. In contrast with a previous work reporting that Meth induces a proinflammatory response in an immortalized microglial cell line [63], our results demonstrated that Meth does not directly cause a proinflammatory phenotype in primary microglia. Likewise, our primary microglia cultures were responsive to LPS, excluding the possibility that the lack of a direct Meth effect could be due to microglia anergy [64]. Nonetheless, and corroborating our findings, Frank and colleagues observed that Meth fails to induce the expression of proinflammatory cytokines in microglial cultures despite upregulating IL-1, IL-6, and TNF in vivo [64]. Similarly, cocaine was also reported to be ineffective in inducing microglial TNF mRNA levels in vitro [65].

As Meth activated microglia in vivo, we tested the hypothesis that this activation could result from an interplay with other cell types. Reactive astrocytes [66] are observed in several models of Meth exposure [33, 67, 68], including human cerebral organoids [69], and are persistently associated with increased neurotoxicity and neuroinflammation, strengthening the likelihood of an astrocyte-mediated microglial response. Astrocytes seem to control immune activation via the secretion of multiple molecular factors [70, 71]; among them, TNF emerged as an essential mediator of brain homeostasis [72]. We demonstrated that Meth increased TNF content in hippocampal astrocytes, suggesting that TNF may play a crucial role in microglia activation by Meth-sensitized astrocytes. Indeed, it has been reported that an

autocrine/paracrine TNF-dependent TNFR1 activation promotes glutamate release from astrocytes [48], while TNF inhibitors strongly reduce glutamate release in cultured astrocytes [73]. In line with this, we also observed that while Meth triggered rapid and sustained glutamate release from astrocytes obtained from WT mice, it failed to do so in astrocytes obtained from TNF KO. In addition, TNF downregulates the glutamate transporter EAAT-2 on astrocytes, compromising glutamate clearance from the extracellular space and promoting excitotoxic glutamate signaling [74, 75].

Excitotoxicity associates positively with the progression of several neurodegenerative diseases [76]. Meth, by acting on the trace amine-associated receptor 1 (TAAR1), induces excitotoxicity through downregulation of EAAT-2 transcription and activity in astrocytes [77]. In this context, our results strongly suggest that glutamate is a critical modulator in Meth-induced microglial activation. Corroborating this hypothesis, we observed that Meth failed to induce microgliosis, reduced anxiety-like behavior and loss of risk-assessment behavior in TNF-deficient mice. Interestingly, TNF-deficient mice were previously reported to self-administer more Meth [78], which according to our data, may also result from reduced astrocyte-microglia reactivity, and not only from increased dopamine availability, as previously suggested [27].

Astrocytes release glutamate through different pathways, including Ca^{2+} -dependent and -independent mechanisms [50]. The ER serves as a major source for astrocytic mobilization of intracellular Ca^{2+} via IP_3R [13, 79]. We evaluated the involvement of IP_3 in Meth-induced glutamate release from astrocytes and confirmed that it occurred in an IP_3 -dependent way. Accordingly, when we administered Meth to $\text{IP}_3\text{R}2$ -deficient mice, microgliosis and behavioral changes were prevented, suggesting that astrocytic $\text{IP}_3\text{R}/\text{Ca}^{2+}$ signaling is required for microglia activation triggered by Meth. Although we focused on the TNF-dependent effect on glutamate release, TNF released from astrocytes can interact with TNFRs present in microglia and further contribute to the microglial activation observed in response to Meth. This fact is in accordance with our RNA-Seq data demonstrating an upregulation of the TNF- α NF- κB signaling pathway in microglia following exposure to Meth.

Astrocytes were also recently demonstrated as critical modulators of the reward system, responding to amphetamine-elicited dopaminergic signaling and regulating excitatory neurotransmission through adenosine receptors [80]. Our results provide further mechanistic insight reinforcing the role of astrocytes in reward and addiction by also controlling microglial reactivity.

Collectively, our findings show that astrocytes cause the activation of microglia in acute Meth-exposure *via* glutamate release in a TNF/ $\text{IP}_3\text{R}2$ - Ca^{2+} -dependent manner (Fig. 5). Understanding how microglial reactivity and neuroinflammation will adapt throughout prolonged exposure to Meth, particularly during withdrawal, will further increase the translational significance of our findings and contribute to identifying novel molecular targets with therapeutic value in psychostimulant abuse.

REFERENCES

1. Thanos PK, Kim R, Delis F, Ananth M, Chachati G, Rocco MJ, et al. Chronic methamphetamine effects on brain structure and function in rats. *PLoS One*. 2016;11:e0155457.
2. Chang X, Sun Y, Zhang Y, Muhai J, Lu L, Shi J. A review of risk factors for methamphetamine-related psychiatric symptoms. *Front Psychiatry*. 2018;9:603.
3. Cadet JL, Bisagno V, Milroy CM. Neuropathology of substance use disorders. *Acta Neuropathol*. 2014;127:91–107.
4. Mszczynska A, Callan SP. Molecular, behavioral, and physiological consequences of methamphetamine neurotoxicity: implications for treatment. *J Pharm Exp Ther*. 2017;362:474–88.
5. Northrop NA, Halpin LE, Yamamoto BK. Peripheral ammonia and blood brain barrier structure and function after methamphetamine. *Neuropharmacology*. 2016;107:18–26.

6. Shaerzadeh F, Streit WJ, Heysieattalab S, Khoshbouei H. Methamphetamine neurotoxicity, microglia, and neuroinflammation. *J Neuroinflammation*. 2018;15:341.
7. Yamamoto BK, Raudensky J. The role of oxidative stress, metabolic compromise, and inflammation in neuronal injury produced by amphetamine-related drugs of abuse. *J Neuroimmune Pharm*. 2008;3:203–17.
8. Cadet JL, Bisagno V. Glial-neuronal ensembles: partners in drug addiction-associated synaptic plasticity. *Front Pharm*. 2014;5:204.
9. Miguel-Hidalgo JJ. The role of glial cells in drug abuse. *Curr Drug Abuse Rev*. 2009;2:72–82.
10. Beardsley PM, Hauser KF. Glial modulators as potential treatments of psychostimulant abuse. *Adv Pharm*. 2014;69:1–69.
11. Araque A, Carmignoto G, Haydon PG, Oliet SH, Robitaille R, Volterra A. Gliotransmitters travel in time and space. *Neuron*. 2014;81:728–39.
12. Tszchentke TM, Schmidt WJ. Glutamatergic mechanisms in addiction. *Mol Psychiatry*. 2003;8:373–82.
13. Bazargani N, Attwell D. Astrocyte calcium signaling: the third wave. *Nat Neurosci*. 2016;19:182–9.
14. Clark KH, Wiley CA, Bradberry CW. Psychostimulant abuse and neuroinflammation: emerging evidence of their interconnection. *Neurotox Res*. 2013;23:174–88.
15. Krasnova IN, Justinova Z, Cadet JL. Methamphetamine addiction: involvement of CREB and neuroinflammatory signaling pathways. *Psychopharmacol (Berl)*. 2016;233:1945–62.
16. Salter MW, Beggs S. Sublime microglia: expanding roles for the guardians of the CNS. *Cell*. 2014;158:15–24.
17. Harms AS, Lee JK, Nguyen TA, Chang J, Ruhn KM, Trevino I, et al. Regulation of microglia effector functions by tumor necrosis factor signaling. *Glia*. 2012;60:189–202.
18. Prinz M, Priller J. Microglia and brain macrophages in the molecular age: from origin to neuropsychiatric disease. *Nat Rev Neurosci*. 2014;15:300–12.
19. Biber K, Moller T, Boddeke E, Prinz M. Central nervous system myeloid cells as drug targets: current status and translational challenges. *Nat Rev Drug Discov*. 2016;15:110–24.
20. Stephenson J, Nutma E, van der Valk P, Amor S. Inflammation in CNS neurodegenerative diseases. *Immunology*. 2018;154:204–19.
21. Subhramanyam CS, Wang C, Hu Q, Dheen ST. Microglia-mediated neuroinflammation in neurodegenerative diseases. *Semin Cell Dev Biol*. 2019;94:112–20.
22. Socodato R, Henriques JF, Portugal CC, Almeida TO, Tedim-Moreira J, Alves RL, et al. Daily alcohol intake triggers aberrant synaptic pruning leading to synapse loss and anxiety-like behavior. *Sci Signal*. 2020;13:eaba5754.
23. ter Horst JP, de Kloet ER, Schachinger H, Oitzl MS. Relevance of stress and female sex hormones for emotion and cognition. *Cell Mol Neurobiol*. 2012;32:725–35.
24. Li X, Zima AV, Sheikh F, Blatter LA, Chen J. Endothelin-1-induced arrhythmogenic Ca^{2+} signaling is abolished in atrial myocytes of inositol-1,4,5-trisphosphate (IP_3)-receptor type 2-deficient mice. *Circ Res*. 2005;96:1274–81.
25. Guerra-Gomes S, Sousa N, Pinto L, Oliveira JF. Functional roles of astrocyte calcium elevations: from synapses to behavior. *Front Cell Neurosci*. 2018;11:427.
26. Thomas DM, Walker PD, Benjamins JA, Geddes TJ, Kuhn DM. Methamphetamine neurotoxicity in dopamine nerve endings of the striatum is associated with microglial activation. *J Pharm Exp Ther*. 2004;311:1–7.
27. Nakajima A, Yamada K, Nagai T, Uchiyama T, Miyamoto Y, Mamiya T, et al. Role of tumor necrosis factor- α in methamphetamine-induced drug dependence and neurotoxicity. *J Neurosci*. 2004;24:2212–25.
28. Krasnova IN, Cadet JL. Methamphetamine toxicity and messengers of death. *Brain Res Rev*. 2009;60:379–407.
29. Galatro TF, Vainchtein ID, Brouwer N, Boddeke E, Eggen BJL. Isolation of microglia and immune infiltrates from mouse and primate central nervous system. *Methods Mol Biol*. 2017;1559:333–42.
30. Socodato R, Portugal CC, Canedo T, Rodrigues A, Almeida TO, Henriques JF, et al. Microglia dysfunction caused by the loss of rhoa disrupts neuronal physiology and leads to neurodegeneration. *Cell Rep*. 2020;31:107796.
31. Andrade EB, Magalhaes A, Puga A, Costa M, Bravo J, Portugal CC, et al. A mouse model reproducing the pathophysiology of neonatal group B streptococcal infection. *Nat Commun*. 2018;9:3138.
32. Portugal CC, Socodato R, Canedo T, Silva CM, Martins T, Coreixas VS, et al. Caveolin-1-mediated internalization of the vitamin C transporter SVCT2 in microglia triggers an inflammatory phenotype. *Sci Signal*. 2017;10:eaa12005.
33. Bortell N, Basova L, Semenova S, Fox HS, Ravasi T, Marcondes MC. Astrocyte-specific overexpressed gene signatures in response to methamphetamine exposure *in vitro*. *J Neuroinflammation* 2017;14:49.
34. Socodato R, Portugal CC, Domith I, Oliveira NA, Coreixas VS, Loliola EC, et al. c-Src function is necessary and sufficient for triggering microglial cell activation. *Glia*. 2015;63:497–511.
35. Koenigsnecht J, Landreth G. Microglial phagocytosis of fibrillar beta-amyloid through a beta1 integrin-dependent mechanism. *J Neurosci*. 2004;24:9838–46.

36. Socodato R, Melo P, Ferraz-Nogueira JP, Portugal CC, Relvas JB. A protocol for FRET-based live-cell imaging in microglia. *STAR Protocols*. 2020;1:100147.
37. Mateus-Pinheiro A, Alves ND, Patrício P, Machado-Santos AR, Loureiro-Campos E, Silva JM, et al. AP2γ controls adult hippocampal neurogenesis and modulates cognitive, but not anxiety or depressive-like behavior. *Mol Psychiatry*. 2017;22:1725–34.
38. Ayata P, Badimon A, Strasburger HJ, Duff MK, Montgomery SE, Loh Y-HE, et al. Epigenetic regulation of brain region-specific microglia clearance activity. *Nat Neurosci*. 2018;21:1049–60.
39. Butovsky O, Jedrychowski MP, Moore CS, Cialic R, Lanser AJ, Gabriely G, et al. Identification of a unique TGF-β-dependent molecular and functional signature in microglia. *Nat Neurosci*. 2014;17:131–43.
40. Hammond TR, Dufort C, Dissing-Olesen L, Giera S, Young A, Wysoker A, et al. Single-cell RNA sequencing of microglia throughout the mouse lifespan and in the injured brain reveals complex cell-state changes. *Immunity*. 2019;50:253–71. e6.
41. Keren-Shaul H, Spinrad A, Weiner A, Matcovitch-Natan O, Dvir-Szternfeld R, Ulland TK, et al. A unique microglia type associated with restricting development of Alzheimer's disease. *Cell*. 2017;169:1276–90. e17.
42. Najera JA, Bustamante EA, Bortell N, Morsey B, Fox HS, Ravasi T, et al. Methamphetamine abuse affects gene expression in brain-derived microglia of SIV-infected macaques to enhance inflammation and promote virus targets. *BMC Immunol*. 2016;17:7–7.
43. Savell KE, Tuscher JJ, Zipperly ME, Duke CG, Phillips RA, Bauman AJ, et al. A dopamine-induced gene expression signature regulates neuronal function and cocaine response. *Sci Adv*. 2020;6:eaba4221.
44. Astarita G, Avanesian A, Grimaldi B, Realini N, Justinova Z, Panlilio LV, et al. Methamphetamine accelerates cellular senescence through stimulation of de novo ceramide biosynthesis. *PLoS One*. 2015;10:e0116961.
45. Liddel SA, Marsh SE, Stevens B. Microglia and astrocytes in disease: dynamic duo or partners in crime? *Trends Immunol*. 2020;41:820–35.
46. Socodato R, Portugal CC, Canedo T, Domith I, Oliveira NA, Paes-de-Carvalho R, et al. c-Src deactivation by the polyphenol 3-O-caffeoylquinic acid abrogates reactive oxygen species-mediated glutamate release from microglia and neuronal excitotoxicity. *Free Radic Biol Med*. 2015;79:45–55.
47. Gonçalves J, Martins T, Ferreira R, Milhazes N, Borges F, Ribeiro CF, et al. Methamphetamine-induced early increase of IL-6 and TNF-α mRNA expression in the mouse brain. *Ann NY Acad Sci*. 2008;1139:103–11.
48. Bezzi P, Domercq M, Brambilla L, Galli R, Schols D, De Clercq E, et al. CXCR4-activated astrocyte glutamate release via TNF-α: amplification by microglia triggers neurotoxicity. *Nat Neurosci*. 2001;4:702–10.
49. Okumoto S, Looger LL, Micheva KD, Reimer RJ, Smith SJ, Frommer WB. Detection of glutamate release from neurons by genetically encoded surface-displayed FRET nanosensors. *Proc Natl Acad Sci USA*. 2005;102:8740–5.
50. Harada K, Kamiya T, Tsuboi T. Gliotransmitter release from astrocytes: functional, developmental, and pathological implications in the brain. *Front Neurosci*. 2015;9:499.
51. Parpura V, Grubisic V, Verkhratsky A. Ca(2+) sources for the exocytotic release of glutamate from astrocytes. *Biochim Biophys Acta*. 2011;1813:984–91.
52. Palmer AE, Jin C, Reed JC, Tsien RY. Bcl-2-mediated alterations in endoplasmic reticulum Ca2+ analyzed with an improved genetically encoded fluorescent sensor. *Proc Natl Acad Sci USA*. 2004;101:17404–9.
53. Gafni J, Munsch JA, Lam TH, Catlin MC, Costa LG, Molinski TF, et al. Xestopongins: potent membrane permeable blockers of the inositol 1,4,5-trisphosphate receptor. *Neuron*. 1997;19:723–33.
54. Verkhratsky A, Matteoli M, Parpura V, Mothet JP, Zorec R. Astrocytes as secretory cells of the central nervous system: idiosyncrasies of vesicular secretion. *EMBO J*. 2016;35:239–57.
55. Schiavo G, Matteoli M, Montecucco C. Neurotoxins affecting neuroexocytosis. *Physiol Rev*. 2000;80:717–66.
56. Petrávic J, Fiacco TA, McCarthy KD. Loss of IP3 receptor-dependent Ca2+ increases in hippocampal astrocytes does not affect baseline CA1 pyramidal neuron synaptic activity. *J Neurosci*. 2008;28:4967–73.
57. Blank T, Prinz M. Microglia as modulators of cognition and neuropsychiatric disorders. *Glia*. 2013;61:62–70.
58. Rooney S, Sah A, Unger MS, Kharitonova M, Sartori SB, Schwarzer C, et al. Neuroinflammatory alterations in trait anxiety: modulatory effects of minocycline. *Transl Psychiatry*. 2020;10:256.
59. Sekine Y, Ouchi Y, Sugihara G, Takei N, Yoshikawa E, Nakamura K, et al. Methamphetamine causes microglial activation in the brains of human abusers. *J Neurosci*. 2008;28:5756–61.
60. Buchanan JB, Sparkman NL, Johnson RW. A neurotoxic regimen of methamphetamine exacerbates the febrile and neuroinflammatory response to a subsequent peripheral immune stimulus. *J Neuroinflammation*. 2010;7:82.
61. Loftis JM, Choi D, Hoffman W, Huckans MS. Methamphetamine causes persistent immune dysregulation: a cross-species, translational report. *Neurotox Res*. 2011;20:59–68.
62. Block ML, Zecca L, Hong JS. Microglia-mediated neurotoxicity: uncovering the molecular mechanisms. *Nat Rev Neurosci*. 2007;8:57–69.
63. Coelho-Santos V, Gonçalves J, Fontes-Ribeiro C, Silva AP. Prevention of methamphetamine-induced microglial cell death by TNF-α and IL-6 through activation of the JAK-STAT pathway. *J Neuroinflammation*. 2012;9:103.
64. Frank MG, Adhikary S, Sobesky JL, Weber MD, Watkins LR, Maier SF. The danger-associated molecular pattern HMGB1 mediates the neuroinflammatory effects of methamphetamine. *Brain Behav Immun*. 2016;51:99–108.
65. Lewitus GM, Konefal SC, Greenhalgh AD, Pribiag H, Augereau K, Stellwagen D. Microglial TNF-α suppresses cocaine-induced plasticity and behavioral sensitization. *Neuron*. 2016;90:483–91.
66. Escartin C, Galea E, Lakatos A, O'Callaghan JP, Petzold GC, Serrano-Pozo A, et al. Reactive astrocyte nomenclature, definitions, and future directions. *Nat Neurosci*. 2021;24:312–25.
67. Narita M, Miyatake M, Narita M, Shibasaki M, Shindo K, Nakamura A, et al. Direct evidence of astrocytic modulation in the development of rewarding effects induced by drugs of abuse. *Neuropsychopharmacology*. 2006;31:2476–88.
68. Du SH, Qiao DF, Chen CX, Chen S, Liu C, Lin Z, et al. Toll-like receptor 4 mediates methamphetamine-induced neuroinflammation through caspase-11 signaling pathway in astrocytes. *Front Mol Neurosci*. 2017;10:409.
69. Dang J, Tiwari SK, Agrawal K, Hui H, Qin Y, Rana TM. Glial cell diversity and methamphetamine-induced neuroinflammation in human cerebral organoids. *Mol Psychiatry*. 2021;26:1194–207.
70. Dong Y, Benveniste EN. Immune function of astrocytes. *Glia*. 2001;36:180–90.
71. Farina C, Aloisi F, Meinl E. Astrocytes are active players in cerebral innate immunity. *Trends Immunol*. 2007;28:138–45.
72. Rossi D. Astrocyte physiopathology: at the crossroads of intercellular networking, inflammation and cell death. *Prog Neurobiol*. 2015;130:86–120.
73. Domercq M, Brambilla L, Pilati E, Marchaland J, Volterra A, Bezzi P. P2Y1 receptor-evoked glutamate exocytosis from astrocytes: control by tumor necrosis factor-α and prostaglandins. *J Biol Chem*. 2006;281:30684–96.
74. Sitcheran R, Gupta P, Fisher PB, Baldwin AS. Positive and negative regulation of EAAT2 by NF-κB: a role for N-myc in TNF-α-controlled repression. *EMBO J*. 2005;24:510–20.
75. Wang Z, Pekarskaya O, Bencheikh M, Chao W, Gelbard HA, Ghorpade A, et al. Reduced expression of glutamate transporter EAAT2 and impaired glutamate transport in human primary astrocytes exposed to HIV-1 or gp120. *Virology*. 2003;312:60–73.
76. Doble A. The role of excitotoxicity in neurodegenerative disease: implications for therapy. *Pharm Ther*. 1999;81:163–221.
77. Cisneros IE, Ghorpade A. Methamphetamine and HIV-1-induced neurotoxicity: role of trace amine associated receptor 1 cAMP signaling in astrocytes. *Neuropharmacology*. 2014;85:499–507.
78. Yan Y, Nitta A, Koseki T, Yamada K, Nabeshima T. Dissociable role of tumor necrosis factor alpha gene deletion in methamphetamine self-administration and cue-induced relapsing behavior in mice. *Psychopharmacol*. 2012;221:427–36.
79. Volterra A, Liaudet N, Savtchouk I. Astrocyte Ca(2+) signalling: an unexpected complexity. *Nat Rev Neurosci*. 2014;15:327–35.
80. Corkrum M, Covelo A, Lines J, Bellocchio L, Pisansky M, Loke K, et al. Dopamine-evoked synaptic regulation in the nucleus accumbens requires astrocyte activity. *Neuron*. 2020;105:1036–47. e5.

ACKNOWLEDGEMENTS

We acknowledge the support of the following i3S Scientific Platforms: Animal Facility, Cell Culture and Genotyping (CCGen), Translational Cytometry Unit (TraCy), and the assistance of Mafalda Rocha (Genomics platform) and Maria Azevedo (ALM platform) and André Maia (BioSciences screening). We also acknowledge our late colleague Rui Appelberg for kindly make TNF KO mice available to us, and the designer Maria Summavielle for her contribution in assembling the figures that illustrate this publication. RS has contributed as first author.

AUTHOR CONTRIBUTIONS

Conception of the work—TC, CCP, RS, JBR, TS; Acquisition, analysis, or interpretation of data for the work—TC, CCP, RS, TOA, AFT, JB, AIS, JDM, SGG, JFO, AM, JBR, TS; Drafting the work or revising it critically—TC, CCP, RS, NS, JFO, JBR, TS; Final approval of the version to be published—TC, CCP, TS. Agreement to be accountable for all aspects of the work in ensuring accuracy and integrity—CCP and TS.

FUNDING

This work was financed by FEDER—Fundo Europeu de Desenvolvimento Regional funds through the COMPETE 2020 - Operational Programme for Competitiveness and Internationalisation (POCI), Portugal 2020, and by Portuguese funds through FCT—Fundação para a Ciência e a Tecnologia/Ministério da Ciência (FCT), Tecnologia e Ensino Superior in the framework of the project POCI-01-0145-FEDER-030647 (PTDC/SAU-TOX/30647/2017) in TS lab. FEDER Portugal (Norte-01-0145-FEDER-000008000008—Porto Neurosciences and Neurologic Disease Research Initiative at I3S, supported by Norte Portugal Regional Operational Programme (NORTE 2020), under the PORTUGAL 2020 Partnership Agreement, through the European Regional Development Fund (ERDF); FCOMP-01-0124-FEDER-021333). CCP and RS hold employment contracts financed by national funds through FCT—in the context of the program-contract described in paragraphs 4, 5, and 6 of art. 23 of Law no. 57/2016, of August 29, as amended by Law no. 57/2017 of July 2019. TC, TOA, AFT, JB, AIS and AM were supported by FCT (SFRH/BD/117148/2016, SFRH/BD/147981/2019, 2020.07188.BD, PD/BD/135450/2017, SFRH/BD/144324/2019, and IF/00753/2014). Work in JBR lab was supported by the FCT project PTDC/ MED-NEU/31318/2017. JFO was also supported by FCT projects PTDC/MED-NEU/31417/2017 and POCI-01-0145-FEDER-016818; Bial Foundation Grants 207/14 and 037/18, by National funds, through FCT - project UIDB/50026/2020; and by the projects NORTE-01-0145-FEDER-000013 and NORTE-01-0145-FEDER-000023, supported by Norte Portugal Regional Operational Programme (NORTE 2020), under the PORTUGAL 2020 Partnership Agreement, through the European Regional Development Fund (ERDF). Funding of i3S Scientific Platforms: Advanced Light Microscopy (ALM), a member of the national

infrastructure PPBI-Portuguese Platform of Bioluminescence (POCI-01-0145-FEDER-022122); and Genomics through GenomePT project (POCI-01-0145-FEDER-022184), supported by COMPETE 2020—Operational Programme for Competitiveness and Internationalization (POCI), Lisboa Portugal Regional Operational Programme (Lisboa2020), Algarve Portugal Regional Operational Programme (CRESC Algarve2020), under the PORTUGAL 2020 Partnership Agreement, through the European Regional Development Fund (ERDF), and by FCT.

COMPETING INTERESTS

The authors declare no competing interests.

ADDITIONAL INFORMATION

Supplementary information The online version contains supplementary material available at <https://doi.org/10.1038/s41386-021-01139-7>.

Correspondence and requests for materials should be addressed to C.C.P. or T.S.

Reprints and permission information is available at <http://www.nature.com/reprints>

Publisher's note Springer Nature remains neutral with regard to jurisdictional claims in published maps and institutional affiliations.